Journal of Science and Technology in Civil Engineering, HUCE, 2025

NUMERICAL INVESTIGATION ON LOCAL BUCKLING CAPACITY OF COLD-FORMED STEEL COMPRESSION MEMBERS MADE OF ADVANCED HIGH STRENGTH STEELS AT ELEVATED TEMPERATURES

Son Tung Vy[a,b,*]

[a]*School of Civil and Environmental Engineering, Queensland University of Technology, George St, Brisbane City, QLD, Australia*
[b]*Faculty of Building and Industrial Construction, Hanoi University of Civil Engineering, 55 Giai Phong road, Bach Mai ward, Hanoi, Vietnam*

Article history:
Received 10/02/2025, Revised 05/6/2025, Accepted 08/7/2025

Abstract

In recent years, the application of advanced high strength steels for fabricating cold-formed steel (CFS) members has been increasingly focused. The knowledge of the load-bearing capacity of CFS members made of these materials at elevated temperatures (in fire conditions) is limited. This research study focuses on the compression capacity of short CFS lipped channel members made of MS1200 martensitic advanced high strength steel sheets (with a nominal yield strength of 1200 MPa) and failing by local buckling at elevated temperatures. Firstly, finite element (FE) models of these CFS members were developed. These FE models were then used to conduct a parametric study, in which the effects of increasing temperatures on the capacity reduction of short CFS lipped channel members made of MS1200 steel sheets were focused. The difference between the capacity reductions due to elevated temperatures of CFS lipped channel members made of G550 high strength steel sheets (with a nominal yield strength of 550 MPa) and MS1200 steel sheets was also discussed. Finally, the direct strength method (DSM) based design rules for CFS compression members at elevated temperatures in the current CFS design standard in Australia and New Zealand (AS/NZS 4600) were assessed using the obtained FE analysis results.

Keywords: cold-formed steel; advanced high strength steel; lipped channel; elevated temperatures; local buckling.

1. Introduction

Cold-formed steel (CFS) lipped channels have been popularly used for compression members, such as columns, wall studs, bracings and roof or floor truss members, in many low-rise and several mid-rise residential building structures in North America, Australia and New Zealand. The common use of G550 high strength steel material (nominal yield strength of 550 MPa [1]) significantly improves the compression capacity of CFS lipped channel members, which has contributed to the increasing application of these members for building structures. Recently, many engineers have expected to apply CFS lipped channel members for compression members with higher capacity and slenderness in many mid-rise buildings. An obstacle is that although G550 steel sheets are used, the commonly used CFS lipped channel members still have limited compression capacities due to their sensitivity to sectional buckling (local and distortional buckling) and low torsional and flexural stiffness. A solution considered in recent years is using advanced high strength steel materials with a

*Corresponding author. *E-mail address:* s.vy@qut.edu.au (Vy, S. T.)

nominal yield strength of up to 1200 MPa for fabricating CFS lipped channel members to upgrade their compression capacities further. It is noted that advanced high strength steel materials have been widely applied in the automotive industry. Different to high strength steel materials, advanced high strength steel materials have a multiphase microstructure containing one or more phases other than ferrite, pearlite, or cementite. This results in higher strength and durability [2–4].

Many research studies [2–9] have been conducted on the mechanical properties of advanced high strength steel sheets and their applications for CFS compression members in recent years. In detail, Yan et al. [2] investigated the deterioration of the mechanical properties, such as yield strength and elastic modulus, of advanced high strength steel materials with nominal yield strengths from 340 MPa to 1200 MPa at elevated temperatures. Their investigations included two types of advanced high strength steel materials: dual-phase (high strength and plasticity) and martensitic (high strength but lower plasticity) steels. Xia et al. [3] proposed stress-strain models for these advanced high strength steel materials at elevated temperatures and after being exposed to fire. Li et al. [4] investigated the mechanical properties of DP500 dual-phase advanced high strength steel with a nominal yield strength of 500 MPa and a nominal ultimate strength of 780 MPa. Besides, some other research studies [5–9] investigated the compression capacities of CFS members and CFS stud walls made of different advanced high strength steel materials at ambient temperatures. No research studies have focused on the behaviour of CFS members made of the mentioned materials at elevated temperatures and fire conditions. Thus, further studies in this field are needed to enable the safe applications of these materials for CFS members.

This research study focuses on the local buckling capacity of short CFS lipped channel members made of MS1200 martensitic advanced high strength steel sheets with increasing temperatures. Firstly, suitable finite element (FE) models were developed using a stress-strain model of MS1200 steel sheets developed by Xia et al. [3]. The FE models were then validated using test results of short CFS channel members made of G550 high strength steel sheets at elevated temperatures, which were tested by Gunalan et al. [10]. Based on the developed FE models, a parametric study was conducted to investigate the effects of high temperatures on the local buckling capacities of typical CFS lipped channel members made of MS1200 steel sheets. Finally, the direct strength method (DSM) based design rules in the CFS design standard in Australia and New Zealand (AS/NZS 4600 [1]) for CFS members at elevated temperatures were summarised and assessed based on the FE analysis results obtained in the parametric study.

2. Finite element modelling

2.1. Details of finite element models

Fig. 1(a) shows a general view of a FE model developed in this study. It included the accurate geometry of a short CFS lipped channel member. All elements of the modelled channel member were simulated via S4R elements, which are 4-node, quadrilateral, stress/displacement shell elements with reduced integration and a large-strain formulation. Meanwhile, 5 mm × 5 mm meshing (Fig. 1(b)) was applied [11, 12]. To simplify the FE model, the corner radius in the channel member was assumed negligibly small and thus ignored [6, 10, 12]. The ratio of member length to section depth was about 3 to ensure that local buckling was the dominant buckling mode and that the local buckling stress was not affected by end boundary conditions [13]. Fixed-ended boundary conditions were applied. Through multi-point constraints (MPC) typed “tie”, both ends of this channel member were constrained to two reference points (RP-1 and RP-2), which were located at the centroids of its ends. All axial and lateral movements and rotations of RP-1 were restrained while the set-up for RP-2 was mostly similar except that the axial movement was not restrained. The compression load was applied

on the modelled CFS channel member by setting the axial movement of RP-2. The end boundary and loading conditions are presented in Fig. 1(c). In this study, all the FE models were developed using a commercial FE software ABAQUS [14].

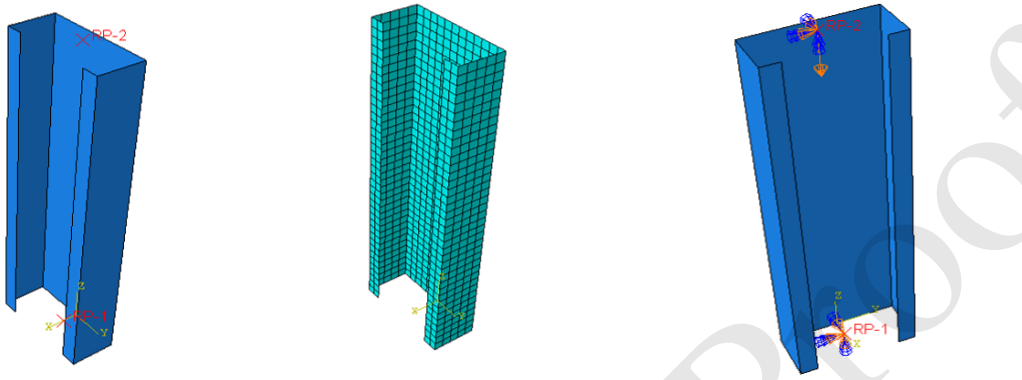

(a) A typical FE model (b) FE mesh (c) End boundary and loading conditions

Figure 1. Overall views of a typical FE model, FE mesh and end boundary and loading conditions

The mechanical properties, including the yield strength ($f_{y,T}$), elastic modulus (E_T) and engineering stress-strain ($\sigma_T - \varepsilon_T$) curves, at elevated temperature (T) of 1 mm thick MS1200 steel sheets were provided in the previous studies [2, 3]. The values of $f_{y,T}$ and E_T are summarised in Table 1, while the engineering stress-strain curves at elevated temperatures are shown in Fig. 2. It should be noted that these curves were based on a simplified stress-strain model proposed by Xia et al. [3] for 1 mm thick MS1200 steel sheets while these curves agreed well with the test results in [2]. All the engineering stress-strain curves ($\sigma_T - \varepsilon_T$) were converted to true stress-strain curves ($\sigma_{T,true} - \varepsilon_{T,true}$) based on Eqs. (1) and (2) before being incorporated into the FE models.

$$\sigma_{T,true} = \sigma_T (1 + \varepsilon_T) \tag{1}$$

$$\varepsilon_{T,true} = \ln (1 + \varepsilon_T) \tag{2}$$

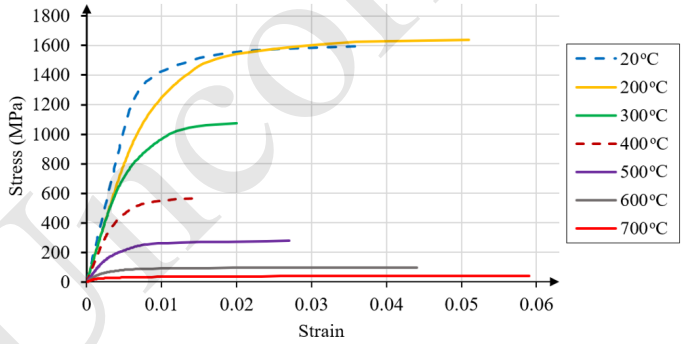

Figure 2. Engineering stress-strain ($\sigma_T - \varepsilon_T$) curves of MS1200 steel sheets

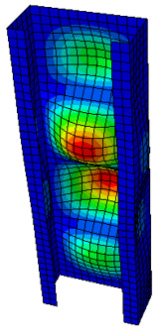

Figure 3. The first local buckling mode of a CFS lipped channel member

As the CFS lipped channel members investigated were sensitive to local buckling mode, local geometric imperfections were incorporated in the FE models. Here, each FE model included two analysis steps. In the first step, eigenvalue buckling analysis was applied to obtain local buckling modes of CFS lipped channel members. In the second step, nonlinear analysis was used to obtain

the compression behaviour, ultimate loads, failure shapes and load-shortening curves of the modelled CFS members. It should be noted that local geometric imperfections based on the first local buckling mode (Fig. 3) given by the first step were incorporated into the nonlinear analysis. The magnitude of the local geometric imperfections was 0.47 × sectional thickness of CFS members [15]. The residual stresses and higher yield strengths at corners of CFS lipped channel sections were ignored based on the proposal of Schafer and Pekoz [16]. In the nonlinear analysis, the General Static solver was applied with a damping factor of 0.0005 and a stabilization factor of 0.005 utilised [11, 12].

Table 1. Mechanical properties of MS1200 steel sheets at elevated temperatures

Mechanical properties	Temperature T (°C)						
	20	200	300	400	500	600	700
$f_{y,T}$	1387.0	1220.6	887.7	513.2	221.9	83.2	27.7
E_T	208609	177318	152285	112649	66755	37550	18775

2.2. *Validation of the developed finite element models*

The FE models developed in this study were validated against test results of short CFS lipped channel members made of 0.95 mm thick G550 high strength steel sheets and failing by local buckling [10]. The simplified stress-strain ($\sigma_T - \varepsilon_T$) curves of 0.95 mm thick G550 steel sheets at elevated temperatures are shown in Fig. 4, which were based on test results of Kankanamge and Mahendran [17] and a stress-strain model proposed by Ranawaka and Mahendran [18] for G550 steel sheets. Figs. 2 and 4 show that except for some differences in terms of the ultimate strains as well as yield and ultimate strengths, the stress-strain curves of MS1200 and G550 steel sheets are highly similar. Therefore, it is reasonable to consider that the compression test results of CFS members made of G550 steel sheets could be used for validating FE models of CFS members made of MS1200 steel sheets.

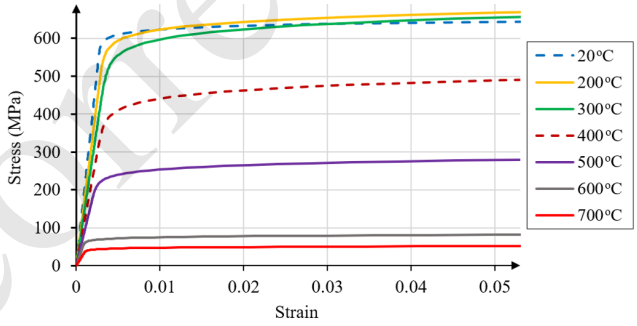

Figure 4. Engineering stress-strain ($\sigma_T - \varepsilon_T$) curves of G550 steel sheets

Table 2 summarises some details of specimens in Gunalan et al. [10], including their lengths (L), section depths (h), flange widths (b), lip widths (d), thicknesses (t), temperatures (T) and the ultimate capacities given by tests and the FE models developed in Section 2.1 ($N_{c,T-Test}$ and $N_{c,T-FEA}$, respectively). The general dimensions and failures of a typical test specimen are shown in Fig. 5. The corner radius in the test specimens was negligibly small [10]. Fig. 6 includes typical load-shortening curves. The high similarities between the test results and the predictions of FE models developed in this study in terms of the ultimate loads, failure shapes and load-shortening curves are presented in Table 2 and Figs. 5 and 6. Therefore, it is concluded that the FE models developed in this study are reliable.

Table 2. Summary of dimensions and capacities of the test specimens in [10]

Specimen	T (°C)	h (mm)	b (mm)	d (mm)	t (mm)	L (mm)	$N_{c,T-Test}$ (kN)	$N_{c,T-FEA}/N_{c,T-Test}$
G550-0.95-20-A	20	62.95	27.65	9.62	0.95	190	53.95	1.04
G550-0.95-200-A	200	63.4	27.75	9.65	0.95	190	52.12	1.02
G550-0.95-300-A	300	63.27	27.7	9.6	0.95	190	47.83	1.02
G550-0.95-400-A	400	63.32	27.61	9.67	0.95	190	36.43	1.00
G550-0.95-500-A	500	63.5	27.75	9.65	0.95	190	21.36	1.02
G550-0.95-600-A	600	63.07	27.72	9.67	0.95	190	6.55	1.07
G550-0.95-700-A	700	63.55	27.55	9.65	0.95	190	4.00	1.10
Average								1.04
COV								0.03

(a) Dimensions of specimens (b) Failures of specimen G550-0.95-700-A in tests (c) Failures of that specimen given by FE models

Figure 5. Details of dimensions of specimens, failures of specimen G550-0.95-700-A in tests, failures of that specimen given by FE models

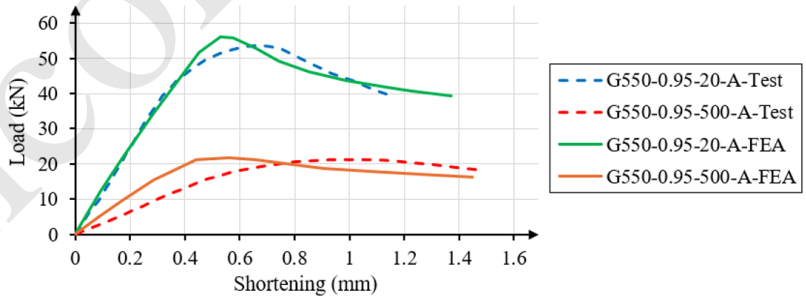

Figure 6. Load-shortening curves of some specimens given by test results and finite element analyses (FEA)

3. Effect of elevated temperatures on the local buckling capacity of CFS compression members made of MS1200 steel sheets

3.1. General

The developed FE models were utilised to investigate the compression capacities of 35 CFS lipped channel members made of MS1200 steel sheets. Their section depths were either 63 mm or 90 mm. In

this Section, the cross-sections of the investigated CFS members were labelled by their dimensions. For example, "C63×28×10×0.75" means that the section depth (h) is 63 mm, flange width (b) is 28 mm, lip width (d) is 10 mm, and thickness (t) is 0.75 mm. The elevated-temperature mechanical properties, including the yield strength ($f_{y,T}$), elastic modulus (E_T) and stress-strain ($\sigma_T - \varepsilon_T$) curves, were assumed as unchanged although the thicknesses were varied. They are presented in Fig. 2 and Table 1. The compression capacities of the investigated CFS members predicted by FE analyses ($N_{c,T-FEA}$) are presented in Table 3. Note that all these CFS members failed by local buckling. Fig. 7 shows the capacity reductions ($N_{c,T-FEA}/N_{c,20-FEA}$) of these CFS members and those made G550 steel sheets in [10].

Table 3. Compression capacities of the investigated CFS members

Cross-section	L (mm)	T (°C)	E_T (MPa)	$f_{y,T}$ (MPa)	$N_{c,T-FEA}$ (kN)	$N_{c,T-FEA}/N_{c,T-DSM}$
C63×28×10×0.75	190	20	208 609	1387.0	60.99	1.14
C63×28×10×0.75	190	200	177 318	1220.6	53.75	1.16
C63×28×10×0.75	190	300	152 285	887.7	40.63	1.13
C63×28×10×0.75	190	400	112 649	513.2	25.32	1.10
C63×28×10×0.75	190	500	66 755	221.9	12.85	1.15
C63×28×10×0.75	190	600	37 550	83.2	5.36	1.10
C63×28×10×0.75	190	700	18 775	27.7	2.10	1.12
C63×28×10×0.95	190	20	208 609	1387.0	97.69	1.21
C63×28×10×0.95	190	200	177 318	1220.6	81.56	1.17
C63×28×10×0.95	190	300	152 285	887.7	63.29	1.17
C63×28×10×0.95	190	400	112 649	513.2	40.62	1.18
C63×28×10×0.95	190	500	66 755	221.9	19.93	1.19
C63×28×10×0.95	190	600	37 550	83.2	7.59	1.05
C63×28×10×0.95	190	700	18 775	27.7	2.90	1.04
C90×40×15×0.75	270	20	208 609	1387.0	68.77	1.16
C90×40×15×0.75	270	200	177 318	1220.6	58.48	1.14
C90×40×15×0.75	270	300	152 285	887.7	45.68	1.14
C90×40×15×0.75	270	400	112 649	513.2	28.56	1.12
C90×40×15×0.75	270	500	66 755	221.9	14.02	1.13
C90×40×15×0.75	270	600	37 550	83.2	5.52	1.02
C90×40×15×0.75	270	700	18 775	27.7	2.35	1.12
C90×40×15×0.95	270	20	208 609	1387.0	102.95	1.15
C90×40×15×0.95	270	200	177 318	1220.6	95.69	1.23
C90×40×15×0.95	270	300	152 285	887.7	68.54	1.14
C90×40×15×0.95	270	400	112 649	513.2	42.17	1.10
C90×40×15×0.95	270	500	66 755	221.9	20.91	1.12

Cross-section	L (mm)	T (°C)	E_T (MPa)	$f_{y,T}$ (MPa)	$N_{c,T-FEA}$ (kN)	$N_{c,T-FEA}/N_{c,T-DSM}$
C90×40×15×0.95	270	600	37 550	83.2	8.40	1.03
C90×40×15×0.95	270	700	18 775	27.7	3.45	1.09
C90×40×15×1.20	270	20	208 609	1387.0	154.77	1.16
C90×40×15×1.20	270	200	177 318	1220.6	135.02	1.16
C90×40×15×1.20	270	300	152 285	887.7	102.27	1.13
C90×40×15×1.20	270	400	112 649	513.2	64.59	1.13
C90×40×15×1.20	270	500	66 755	221.9	31.87	1.14
C90×40×15×1.20	270	600	37 550	83.2	13.23	1.09
C90×40×15×1.20	270	700	18 775	27.7	5.11	1.09
Maximum						1.23
Minimum						1.02
Average						1.13
COV						0.04

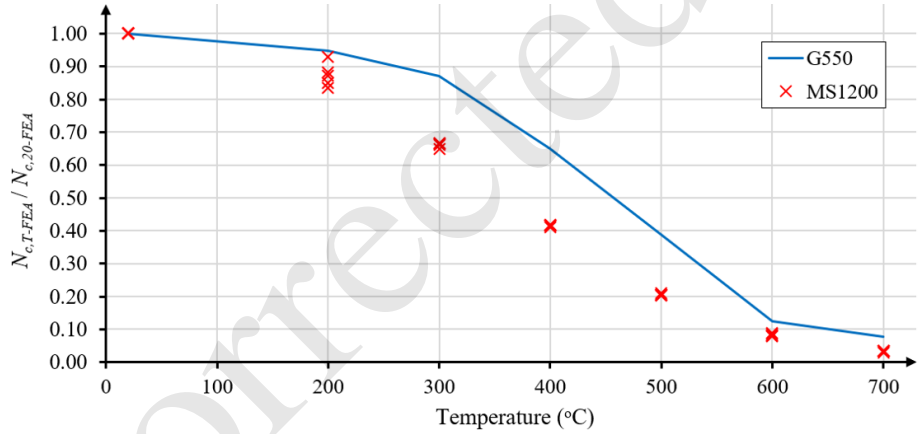

Figure 7. Capacity reductions of CFS members made of MS1200 and G550 steel sheets at elevated temperatures

3.2. Discussions

Fig. 7 and Table 3 highlight that with increasing temperatures, the compression capacities of CFS lipped channel members made of MS1200 steel sheets and failing by local buckling were reduced. At 200 °C, their capacities slightly decreased by around 15%. From 200 °C to 600 °C, their capacities significantly reduced from around 85% to about 10% of their capacities at ambient temperature (20 °C). It is interesting that in this period, the capacity reduction versus temperature relationship was nearly linear. From 600 °C to 700 °C, their compression capacities were gradually reduced to about 5% of their capacities at ambient temperature (20 °C).

At ambient temperature (20 °C), the compression capacity of specimens G550-0.95-20-A made of G550 steel sheets (Table 2) was lower than that of specimen C63×28×10×0.95 made of MS1200 steel sheets (Table 3) by about 80% although these specimens had the same cross-sections and lengths and both failed by local buckling. This meant that using MS1200 could increase the local buckling

capacity of CFS members. As shown in Fig. 7, the compression capacity reduction of CFS lipped channel members made of MS1200 steel sheets was considerably faster than those made of G550 high strength steel sheets, especially during the period from 200 °C to 600 °C. In conclusion, although the use of MS1200 steel could result in the higher compression capacity of CFS lipped channel members failing by local buckling, their performance at elevated temperatures could be worse than the corresponding CFS members made of G550 steel sheets.

4. Design rules

4.1. Direct strength method for the local buckling capacity of CFS compression members at elevated temperatures

Following the direct strength method (DSM) in AS/NZS 4600 [1] and AISI S100 [13], the compression capacity of a CFS member at ambient temperatures is determined as the minimum of the global, local and distortional buckling capacities (N_{ce}, N_{cl} and N_{cd}, respectively). N_{ce} is determined by Eqs. (3) to (5) while N_{cl} and N_{cd} are defined by Eqs. (6) to (11). N_y and N_{oc} are the yield capacity and the minimum of the elastic compression member buckling loads in flexural, torsional, and flexural-torsional buckling. These values can be calculated using appropriate numerical equations in AS/NZS 4600 [1] and AISI S100 [13]. Besides, N_{od} and N_{ol} are the elastic buckling loads in distortional and local buckling modes, respectively, which can be determined using finite strip programs such as CUFSM [19]. To calculate the compression capacity ($N_{c,T-DSM}$) of a CFS lipped channel member at elevated temperatures (T), the same equations and finite strip analyses are applied but with the deteriorated mechanical properties (E_T and $f_{y,T}$) at elevated temperatures. In this study, since the investigated CFS members failed by local buckling, only Eqs. (3) to (8) were assessed.

$$\text{For } \lambda_c \le 1.5, \qquad N_{ce} = \left(0.658^{\lambda_c^2}\right) N_y \tag{3}$$

$$\text{For } \lambda_c > 1.5, \qquad N_{ce} = \left(\frac{0.877}{\lambda_c^2}\right) N_y \tag{4}$$

$$\lambda_c = \sqrt{\frac{N_y}{N_{oc}}} \tag{5}$$

$$\text{If } \lambda_l \le 0.776, \qquad N_{cl} = N_{ce} \tag{6}$$

$$\text{If } \lambda_l > 0.776, \qquad N_{cl} = \left[1 - 0.15\left(\frac{N_{ol}}{N_{ce}}\right)^{0.4}\right]\left(\frac{N_{ol}}{N_{ce}}\right)^{0.4} N_{ce} \tag{7}$$

$$\lambda_l = \sqrt{\frac{N_{ce}}{N_{ol}}} \tag{8}$$

$$\text{If } \lambda_d \le 0.561, \qquad N_{cd} = N_y \tag{9}$$

$$\text{If } \lambda_d > 0.561, \qquad N_{cd} = \left[1 - 0.25\left(\frac{N_{od}}{N_y}\right)^{0.6}\right]\left(\frac{N_{od}}{N_y}\right)^{0.6} N_y \tag{10}$$

$$\lambda_d = \sqrt{\frac{N_y}{N_{od}}} \tag{11}$$

4.2. Discussions

Table 3 shows that the compression capacities of CFS lipped channel members made of MS1200 steel sheets and failing by local buckling at elevated temperatures given by FE analyses ($N_{c,T-FEA}$)

were higher than those predicted by the DSM design rules in AS/NZS 4600 [1] ($N_{c,T-DSM}$) by about 2% to 23%. This proved that the DSM design rules in AS/NZS 4600 [1] were conservative for predicting the compression capacities of the mentioned CFS members. Therefore, these design rules are recommended for designing the mentioned CFS members subjected to uniformly high temperatures in fire conditions, such as those used as CFS columns in fire conditions or those used as CFS studs in CFS stud walls exposed to fire on both sides [20].

5. Conclusions

In this study, the local buckling capacities of CFS lipped channel compression members made of MS1200 steel sheets at elevated temperatures were assessed using many FE analysis results. The FE analyses were validated using suitable test results in an earlier study [10]. The FE analysis results unveiled that although using MS1200 steel sheets for fabricating CFS lipped channel members can significantly improve their local buckling capacity, their performance at elevated temperatures can deteriorate. Further, the DSM design rules in AS/NZS 4600 [1] were proven as could conservatively predict the local buckling capacities of the investigated CFS members.

The FE models developed in this study were validated based on tests of CFS members made of G550 high strength steel sheets and reasonable assumptions. For safer design of CFS members made of MS1200 steel sheets, future experimental studies on these members are recommended.

References

[1] AZ/NZS 4600 (2018). *Cold-formed steel structures*. Sydney, Australia.

[2] Yan, X., Xia, Y., Blum, H. B., Gernay, T. (2020). Elevated temperature material properties of advanced high strength steel alloys. *Journal of Constructional Steel Research*, 174:106299.

[3] Xia, Y., Yan, X., Gernay, T., Blum, H. B. (2022). Elevated temperature and post-fire stress-strain modeling of advanced high-strength cold-formed steel alloys. *Journal of Constructional Steel Research*, 190: 107116.

[4] Li, H.-T., Xu, C.-Y., Zhang, J.-H., Li, H. (2025). Elevated temperature material properties of cold-formed advanced high strength steel channel sections. *Journal of Constructional Steel Research*, 226:109183.

[5] Foroughi, H., Schafer, B. W. (2017). Simulation of conventional cold-formed steel sections formed from advanced high strength steel (AHSS). In *Proceedings of the Annual Stability Conference, Structural Stability Research Council*, San Antonio, Texas, USA.

[6] Ding, C., Xia, Y., Akchurin, D., Li, Z., Blum, H., Schafer, B. W. (2022). Simulation of compressive strength of wall studs cold-formed from advanced high strength steels. In *Proceedings of Structural Stability Research Council Conference*, Atlanta, Georgia, USA.

[7] Zhang, J.-H., Xu, S., Wang, J., Wang, F. (2024). Test, numerical investigation and design of perforated advanced high-strength steel I-shaped built-up compression members. *Engineering Structures*, 314: 118246.

[8] Zhang, J.-H., Wang, J., Xu, S., Wang, F. (2024). Testing, numerical modeling and design of perforated advanced high-strength steel channel section columns. *Journal of Constructional Steel Research*, 214: 108440.

[9] Akchurin, D., Torabian, S., Schafer, B. W. (2025). High-strength cold-formed steel stiffened channel section: Axial compressive strength and initial geometric imperfections. *Thin-Walled Structures*, 206: 112604.

[10] Gunalan, S., Bandula Heva, Y., Mahendran, M. (2015). Local buckling studies of cold-formed steel compression members at elevated temperatures. *Journal of Constructional Steel Research*, 108:31–45.

[11] Vy, S. T., Mahendran, M. (2024). Design of slender built-up back-to-back CFS channel columns with pinned warping-free ends. *Journal of Structural Engineering (ASCE)*, 150(8):04024092.

[12] Vy, S. T., Vu, A. T. (2025). Fire resistance behaviour of non-load bearing LSF walls with restrained thermal elongation. *Journal of Constructional Steel Research*, 224:109145.

[13] AISI S100 (2016). *North American specification for the design of cold-formed steel structural members*. American Iron and Steel Institute, USA.
[14] Dassault Systemes (2022). *ABAQUS*. Providence, RI, USA.
[15] Zeinoddini, V., Schafer, B. (2012). Simulation of geometric imperfections in cold-formed steel members using spectral representation approach. *Thin-Walled Structures*, 60:105–117.
[16] Schafer, B., Peköz, T. (1998). Computational modeling of cold-formed steel: characterizing geometric imperfections and residual stresses. *Journal of Constructional Steel Research*, 47(3):193–210.
[17] Kankanamge, N. D., Mahendran, M. (2011). Mechanical properties of cold-formed steels at elevated temperatures. *Thin-Walled Structures*, 49(1):26–44.
[18] Ranawaka, T., Mahendran, M. (2009). Experimental study of the mechanical properties of light gauge cold-formed steels at elevated temperatures. *Fire Safety Journal*, 44(2):219–229.
[19] Li, Z., Schafer, B. W. (2010). Buckling analysis of cold-formed steel members with general boundary conditions using CUFSM: conventional and constrained finite strip methods. In *Proceedings of the 20th International Specialty Conference on Cold-Formed Steel Structures*, Missouri, USA.
[20] Vy, S. T., Ariyanayagam, A., Mahendran, M. (2024). Behaviour and design of CFS stud walls under both sides fire exposure. *Thin-Walled Structures*, 197:111619.